

# Sodium Mesoxalate as Sacrificial Salt for Biomass-Derived Hard Carbon // Polyanionic Cathode Na-Ion Full Cells

Nekane Nieto,\* Marilena Mancini, Alexander Lopez-Urionabarrenechea, Peter Axmann, Margret Wolfahrt-Mehrens, Maider Iturrondobeitia, Verónica Palomares, and Teófilo Rojo

Up to date, research on sodium-ion batteries (SIBs) has primarily focused on half-cell configurations, a crucial but preliminary step in evaluating suitable materials for full-cell SIBs. To date, the literature on hard carbon (HC)-based full-cell SIBs remains limited, and the irreversibility associated with the first cycle of HC anodes presents a significant challenge for the commercialization of hard carbon-based SIBs. This work evaluates sodium mesoxalate as a sacrificial salt (SS) in the cathode to compensate for biomass-based hard carbon first cycle irreversibility in two full-cell systems *versus*  $\text{Na}_3\text{V}_2(\text{PO}_4)_3@\text{C}$  and  $\text{Na}_3\text{V}_2\text{O}_2(\text{PO}_4)_2\text{F}@\text{C}$ . This sacrificial salt is selected due to its nonflammability, low cost, and ease of

dehydration. Full-cell studies utilizing the sacrificial salt-containing cathodes and biomass-derived hard carbon anodes demonstrate to achieve outstanding specific capacity and rate capability at low and moderate rates (from 9 to 130 mA g<sup>-1</sup>) for the fluorophosphate cell chemistry but poorer electrochemical results for the NASICON-based system. Finally, Life Cycle Assessment methodology is applied to the sacrificial salt containing full-cells to evaluate and compare the environmental footprint of these SS full-cells based on a sustainable anode with polyanionic cathode chemistries.

## 1. Introduction

Sodium-ion batteries (SIBs) are now poised for commercialization, with companies like HiNa and CATL in China, Tiamat in France, Natron Energy in the USA, and Faradion in the UK at the forefront of bringing SIBs to market.<sup>[1–5]</sup> Nonetheless, despite this significant progress, most SIB research remains limited to half-cells, hindering a complete understanding of real-world performance in full-cell configurations. Hard carbon (HC) stands as the most prominent anode material for sodium-ion batteries (SIBs).<sup>[6]</sup> Its structure features a disordered carbon framework that contains high amounts of closed micropores and it can be synthesized from a wide range of low-cost precursors, such as biomass waste.<sup>[7]</sup> Leveraging biomass waste as hard carbon in sodium-ion battery production promotes a circular economy and develops the bioeconomy. This

sustainable approach not only helps the transition away from fossil fuels but also transforms bio-based waste into valuable battery materials.<sup>[8]</sup> A previous investigation into HC derived from sunflower seed shells revealed a material characterized by a high degree of closed microporosity and an expanded interlayer space within the graphitic structure. This combination of features endowed the hard carbon with superior electrochemical properties compared to other samples produced, consistent with the highest performance values reported in the literature for HCs derived from biomass waste.<sup>[9]</sup> This work addresses the assembly of full-cell SIBs by using this sunflower seed shells-derived hard carbon *versus* two polyanionic cathode materials: NASICON-type  $\text{Na}_3\text{V}_2(\text{PO}_4)_3$  and  $\text{Na}_3(\text{VO})_2(\text{PO}_4)_2\text{F}$ .<sup>[10–17]</sup> These compounds are appealing cathode materials due to their high operating voltages, structural stability, and excellent cyclability.<sup>[18–22]</sup>

N. Nieto

Institute for Applied Materials – Energy Storage Systems (IAM-ESS)  
Karlsruhe Institute of Technology (KIT)  
Hermann-von-Helmholtz-Platz 1, 76344 Eggenstein-Leopoldshafen,  
Germany  
E-mail: nekane.nieto@kit.edu

N. Nieto, V. Palomares, T. Rojo  
Organic and Inorganic Chemistry Department  
Science and Technology Faculty  
University of the Basque Country UPV/EHU  
P.O. Box 644, 48080 Bilbao, Spain

M. Mancini, P. Axmann, M. Wolfahrt-Mehrens  
Zentrum für Sonnenenergie-und Wasserstoff-Forschung Baden-Württemberg (ZSW)  
Helmholtzstraße 8, 89081 Ulm, Germany

A. Lopez-Urionabarrenechea  
Chemical and Environmental Engineering Department  
University of the Basque Country UPV/EHU  
Plaza Ingeniero Torres Quevedo 1, 48013 Bilbao, Spain

M. Iturrondobeitia

Life Cycle Thinking Group  
Department of Graphic Design and Engineering Projects  
University of the Basque Country UPV/EHU  
Plaza Ingeniero Torres Quevedo 1, 48013 Bilbao, Spain

V. Palomares

BCMaterials, Basque Center for Materials Applications and Nanostructures  
UPV/EHU Science Park  
48940 Leioa, Spain

 Supporting information for this article is available on the WWW under <https://doi.org/10.1002/batt.202500252>

 © 2025 The Author(s). *Batteries & Supercaps* published by Wiley-VCH GmbH. This is an open access article under the terms of the Creative Commons Attribution License, which permits use, distribution and reproduction in any medium, provided the original work is properly cited.

The first issue to be solved for the development of practical hard carbon-based SIBs is the formation of the solid electrolyte interphase (SEI) on the anode during the initial cycle. This phenomenon presents a major hurdle for the widespread commercial adoption of hard carbon anodes in sodium-ion batteries. Addressing this limitation is crucial for enabling the widespread industrial use of biomass-derived materials.<sup>[23]</sup> The use of sacrificial salts (SS) presents a promising strategy by effectively counteracting sodium deficiencies arising from surface reactions.<sup>[24]</sup> This approach has been demonstrated to be low cost and compatible with electrode manufacturing processes, and to enhance specific capacity and safety. While various SSs have been investigated, each presents inherent limitations.  $\text{Na}_3\text{N}$  poses significant safety hazards due to its explosive nature.  $\text{Na}_3\text{P}$ , despite its potential, is incompatible with current manufacturing processes due to its high toxicity, flammability, and the stringent requirement for handling under inert conditions.<sup>[25–27]</sup>  $\text{Na}_2\text{CO}_3$  has also been used as SS, but, despite its solubility in water, it presents high decomposition potential; thus, it seems more adequate for higher voltage cathodes.<sup>[28]</sup> Furthermore, while  $\text{Na}_2\text{C}_4\text{O}_4$  offers an environmentally friendly and efficient alternative, the high production cost of squaric acid, its precursor, remains a significant obstacle.<sup>[10,11,29]</sup> Sodium mesoxalate, commercially available as sodium mesoxalate monohydrated ( $\text{Na}_2\text{C}_3\text{O}_5 \cdot \text{H}_2\text{O}$ ), emerges as a promising alternative sacrificial salt for SIBs. Although a preliminary drying step is necessary to remove the inherent water content, it offers several key advantages. Notably, sodium mesoxalate exhibits a suitable oxidation potential of  $\approx 4.00$  V versus  $\text{Na}^+/\text{Na}$ , it does not present either high cost or toxicity, and it is stable in dry atmosphere and compatible with dry room electrode processing and possesses an environmentally benign profile.<sup>[12]</sup>

Additionally, the transition from half- to full-cells presents challenges related to achieving optimal electrode capacity balance, which needs careful consideration of the mass loading and thickness of both the anode and cathode.<sup>[30]</sup> While maximizing energy density is a crucial objective, potential safety risks associated with sodium deposition, such as thermal runaway, short circuits, and ultimately, fire or explosion, must be carefully addressed.<sup>[13,14]</sup> A critical initial step toward realizing practical full-cells that deliver optimal material performance involves optimizing the negative areal capacity/positive areal capacity (N/P) ratio, where areal capacity is measured in  $\text{mAh cm}^{-2}$ .<sup>[15]</sup> Calculating the N/P ratio requires determining the practical specific capacity after the formation cycle ( $\text{mAh cm}^{-2}$ ) of both the negative and positive electrodes, as well as their respective mass loadings ( $\text{g cm}^{-2}$ ). An N/P ratio below 1 indicates an excess of positive electrode material. This imbalance leads to the deposition of metallic sodium on the hard carbon anode due to insufficient anode capacity to accommodate all the available  $\text{Na}^+$  ions. Conversely, an N/P ratio above 1 signifies a relative abundance of the negative electrode. In the case of hard carbon anodes, a high N/P ratio often results in the preferential utilization of the sloping voltage region, leading to limited or negligible utilization of the low-voltage plateau. This inefficient utilization of the hard carbon anode significantly impacts both energy density and Initial Coulombic Efficiency (ICE) of the full-cell.<sup>[16,17]</sup>

At this stage of the investigation, where the focus moves to full-cell systems, a thorough evaluation of a battery system must consider the environmental impact of the materials used. In this regard, Life Cycle Assessment (LCA) methodology, following ISO 14040 standards, is suitable for guiding decision-making in the design of new batteries, as it has been demonstrated in the literature.<sup>[31–35]</sup> To sum up, this research investigates the feasibility of assembling fully operative hard carbon-based SIBs without any presodiation step and enhancing their electrochemical performance by incorporating an additive into the positive material. Full-cells were assembled using sunflower seed shells-derived hard carbon as the anode and two different polyanionic compounds as cathodes ( $\text{Na}_3\text{V}_2(\text{PO}_4)_3@\text{C}$  and  $\text{Na}_3\text{V}_2\text{O}_2(\text{PO}_4)_2\text{F}@\text{C}$ ). The study evaluates the performance of these full-cells using two strategies: precycling the hard carbon anode before full-cell assembly to generate the SEI and the addition of sodium mesoxalate into the cathode. Moreover, a life cycle assessment study is performed on the two cell chemistries in order to compare the environmental impact of the proposed SIBs.

## 2. Results and Discussion

The diffractograms of  $\text{Na}_3\text{V}_2(\text{PO}_4)_3@\text{C}$  and  $\text{Na}_3\text{V}_2\text{O}_2(\text{PO}_4)_2\text{F}@\text{C}$  are displayed in Figure 1 together with the diffraction maxima corresponding to PDF-file card numbers 01-078-7289 and 01-083-7199, respectively.<sup>[36–38]</sup> In both cases, a comparison with literature X-ray diffraction (XRD) diagrams shows that the synthesis of the pure materials was accomplished by obtaining the desired compounds. Concerning the morphology of the prepared NVP sample, inset in Figure 1a, it is made of 2–3  $\mu\text{m}$  size particles that gather forming bigger size agglomerates of about 5–7  $\mu\text{m}$ . Furthermore, the composite material was found to contain 7 wt.% carbon, as determined by elemental analysis, but this carbon was not distinguished in the micrograph, due to its low mass percentage. On the contrary, the micrograph of FP material, inset in Figure 1b, shows that the particles of the polyanionic compound are around 1–3  $\mu\text{m}$  size and tend to agglomerate into bigger particles around a 4–7  $\mu\text{m}$  range. Moreover, the carbon content of the composite material was determined to be 14 wt.% through elemental analysis but this carbon is not easily discerned in the micrograph.

The electrochemical performance of the two different cathode formulations used (with and without sodium mesoxalate) was assessed by the evaluation of the cathodes of both active material families,  $\text{Na}_3\text{V}_2(\text{PO}_4)_3@\text{C}$  and  $\text{Na}_3\text{V}_2\text{O}_2(\text{PO}_4)_2\text{F}@\text{C}$  in half-cells (Figure 2). This way the impact of the sacrificial salt on the working voltage or the practical specific capacity was analyzed. The electrochemical profiles of both electrodes, NVP and NVP\_S, exhibit the characteristic shape of NASICON-type polyanionic compounds with a plateau around 3.40 V, that decreases in the discharge step to  $\approx 3.30$  V due to polarization. In the case of NVP\_S electrode (Figure 2c), a small feature associated with the presence of  $\text{Na}_3\text{V}_3(\text{PO}_4)_4$  material can be found around 3.80 V. This compound is an electroactive impurity that reacts at 3.90 V versus  $\text{Na}^+/\text{Na}$ .<sup>[39]</sup> It must be noted that, in the case of the electrodes containing sacrificial salt, (S), a different protocol is carried

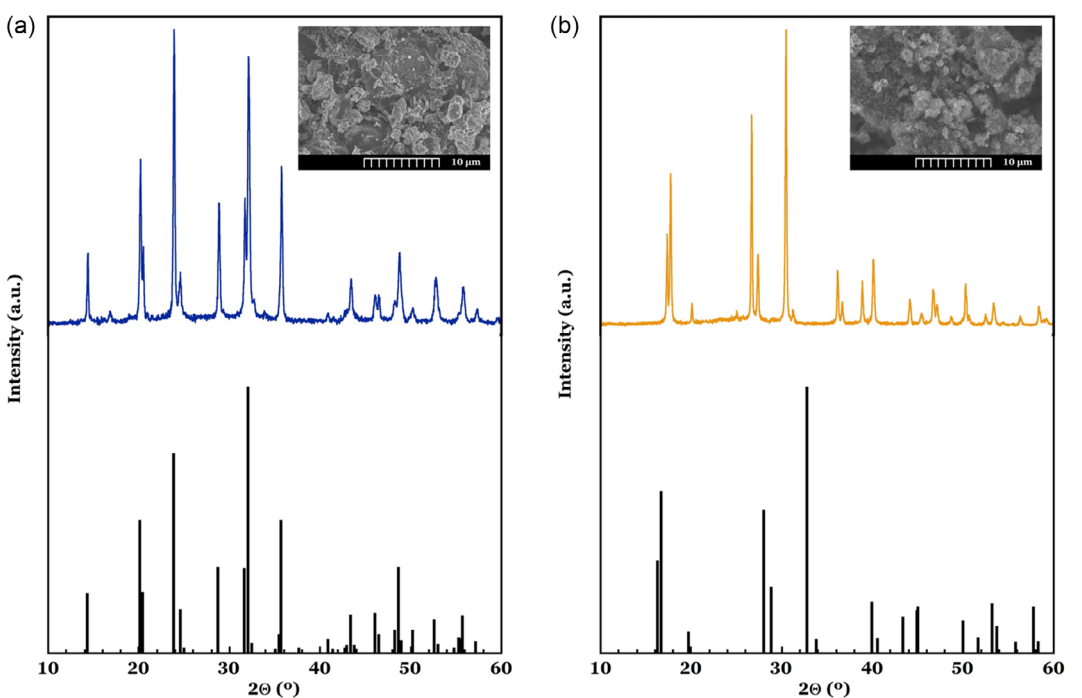


**Figure 1.** SEM micrographs and XRD diffractograms of the prepared a)  $\text{Na}_3\text{V}_2(\text{PO}_4)_3@\text{C}$  (blue) and b)  $\text{Na}_3\text{V}_2\text{O}_2(\text{PO}_4)_2\text{F}@\text{C}$  (orange), in comparison with the ones in literature (black).

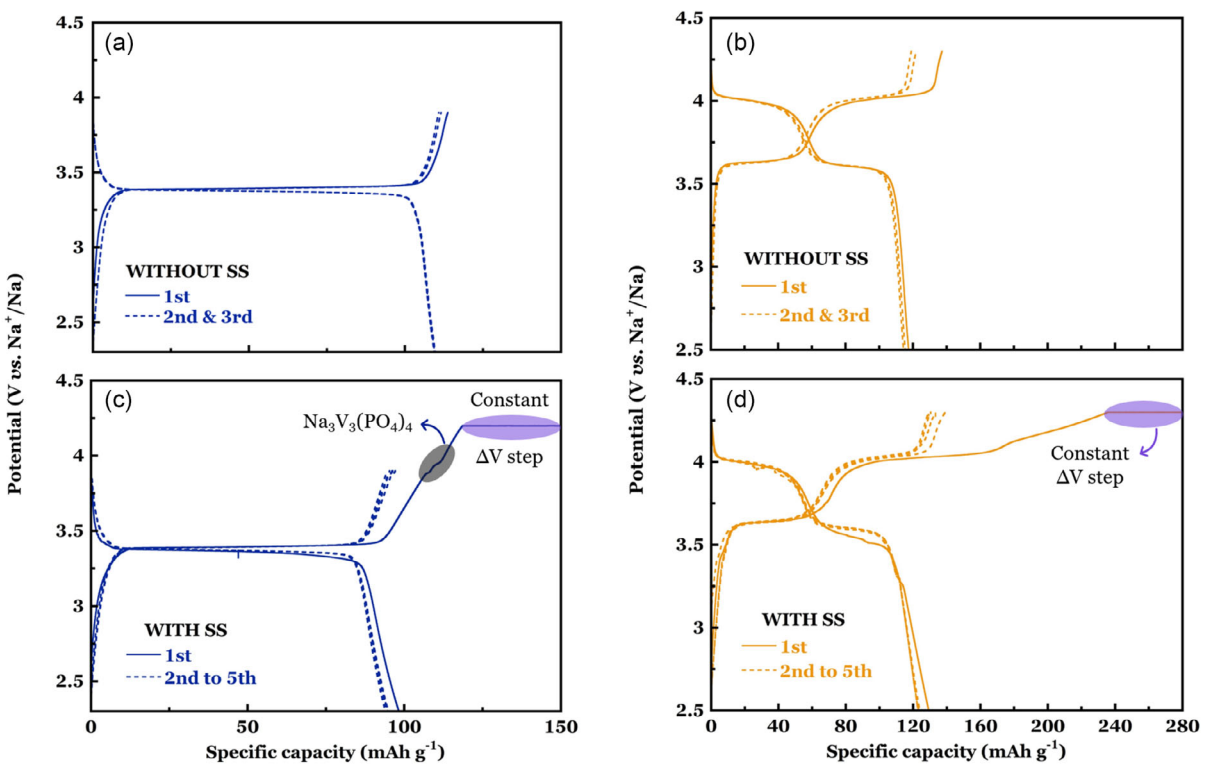


**Figure 2.** Galvanostatic profiles of  $\text{Na}_3\text{V}_2(\text{PO}_4)_3@\text{C}$  and  $\text{Na}_3\text{V}_2\text{O}_2(\text{PO}_4)_2\text{F}@\text{C}$  a,b) without and c,d) with sacrificial salt after several cycles at  $9 \text{ mA g}^{-1}$ , respectively.

out in the first charge, with an extra constant voltage step to decompose sodium mesoxalate at  $4.00 \text{ V}$  versus  $\text{Na}^+/\text{Na}$ . This wider potential window in the first cycle makes  $\text{Na}_3\text{V}_3(\text{PO}_4)_4$

impurity presence noticeable. In terms of specific capacity, NVP\_S shows about 10% lower  $C_{sp}$  compared to NVP cathode (Figure 2a). This could be due to the low conductive properties

of the sacrificial salt despite the low amount of this element in the electrode formulation, only  $\approx 12\%$  of the cathode electrode, and its mixture with Ketjen Black additive. In spite of the lower specific capacity, the use of sodium additive can be beneficial, as it can simplify full-cell assembly, avoiding the electrochemical presodiation of the anode and disassembly of the previous cell.

In contrast, the electrochemical profiles of the cathodes from the fluorophosphate family, FP and FP\_S, (Figure 2b and d, respectively) exhibit the characteristic shape of  $\text{Na}_3\text{V}_2\text{O}_{2x}(\text{PO}_4)_2\text{F}_{3-2x}$  compounds with two plateaus around 3.60 V and 4.00 V versus  $\text{Na}^+/\text{Na}$ , together with the extra feature at 4.00 V that corresponds to sodium mesoxalate decomposition for FP\_S. The discharge curves registered for both FP and FP\_S cathodes are similar, without significant fluctuations of working voltage, specific capacity, or curve shape. These half-cell measurements assess the same electrochemical performance for the FP and FP\_S cathodes. The electrodes assessment was taken as favorable enough to perform the necessary electrochemical tests on two kinds of sunflower seed shells-derived hard carbon-based full-cell systems, the full-cells prepared by pairing a presodiated hard carbon anode to a conventional NVP or FP cathode, versus the full-cells assembled by coupling a fresh hard carbon anode with a cathode containing sacrificial salt (NVP\_S or FP\_S). Electrochemical curves corresponding to the anode presodiation are included in Figure S1, Supporting Information, and experimental details about this step are included in the Experimental Section. Figure 3 depicts the charge–discharge profiles of the HC // NVP and HC // FP presodiated full-cell batteries (Figure 3a,b) and HC // NVP\_S and HC // FP\_S containing sacrificial salt full-cells at different current densities (Figure 3c,d). As previously discussed, calculating the N/P ratio necessitates determining

the practical specific capacity following the formation cycle. This involves half-cell measurements of both the negative and positive electrodes (with and without sacrificial salt), along with their respective mass loadings. The objective of the N/P ratio is to achieve a mass balance between the negative and positive electrodes, with a target value of  $\approx 1.10$ .

In the case of the presodiated full-cells (Figure 3a,b), the cells were disassembled after cycling and the presodiated anodes were paired with the NVP and FP cathodes with mass balances of 1.05 and 1.66, respectively. On the other hand, HC // NVP\_S and HC // FP\_S (Figure 3c,d) containing sodium mesoxalate used mass balances of negative to positive areal capacity of 1.08 and 1.11, respectively. In comparison to half-cell measurements (Figure 2a,b), the HC // NVP presodiated full-cell system (Figure 3a) did not display the typical plateau observed in NASICON-type polyanionic compounds, which is around 3.40 V. The same plateau absence was observed in HC // FP presodiated full-cell (Figure 3b) expected in  $\text{Na}_3\text{V}_2\text{O}_{2x}(\text{PO}_4)_2\text{F}_{3-2x}$  family of compounds around 3.60 V and 4.00 V versus  $\text{Na}^+/\text{Na}$ . This is due to the hard carbon anode contribution to the full-cell electrochemical profile, with its sloppy curve shape. As these electrochemical tests were performed on two-electrode configuration, there are no plots showing separate anode and cathode contributions.

Concerning the specific capacity values obtained, no performance improvement is observed for NVP full-cells when adding the sacrificial salt (Figure 3a,c), with around  $80 \text{ mAh g}^{-1}$  in 9 and  $26 \text{ mA g}^{-1}$  current densities, while showing a marked decrease at high-rate ( $130 \text{ mA g}^{-1}$ ). Moreover, none of the NVP full-cells achieves the  $C_{sp}$  value obtained for the conventional cathodes in half-cells, that is close to  $110 \text{ mAh g}^{-1}$ <sup>[40,41]</sup>. This

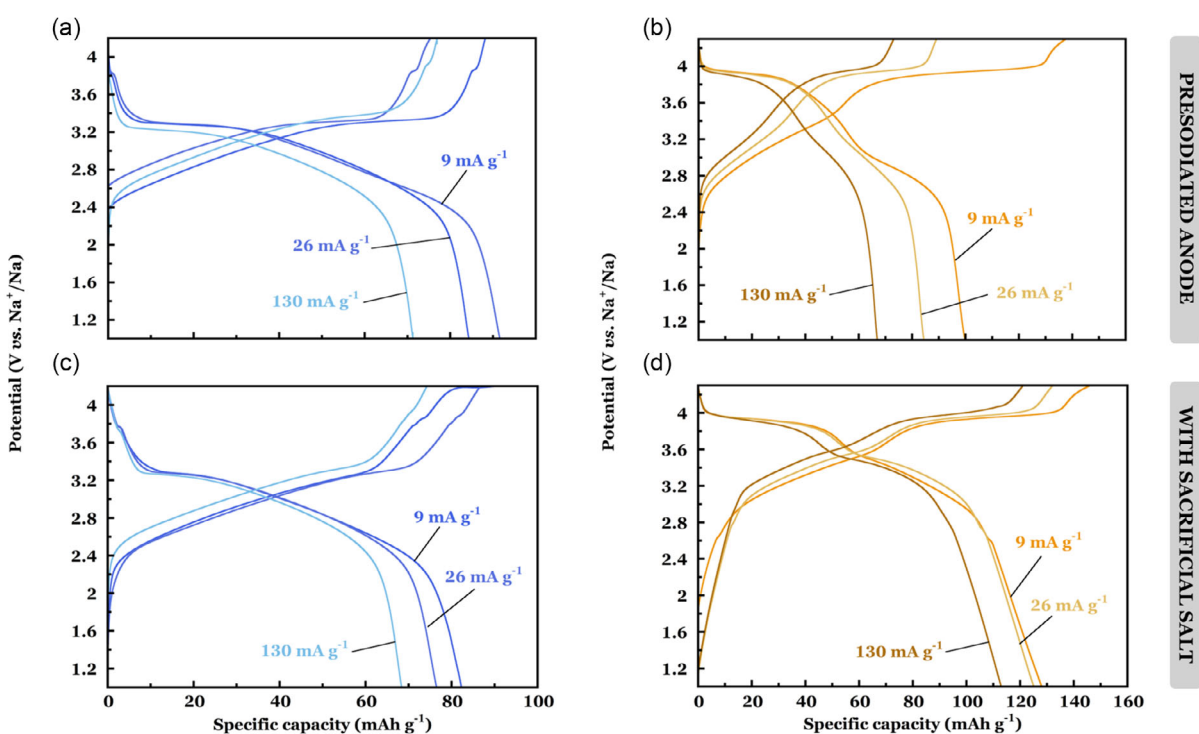


**Figure 3.** Electrochemical performance of a,b) HC // NVP and HC // FP presodiated full-cells and c,d) HC // NVP\_S and HC // FP\_S full-cells with the cathode containing sacrificial salt at different current densities, respectively.

underperformance of the NVP\_S-based full-cells can be related to the lower performance of the sodium mesoxalate containing cathode itself, probably due to the isolating nature of the added sacrificial salt. Further research would be needed for this cell chemistry in order to minimize the sacrificial salt proportion in the cathode formulation and also to optimize the necessary negative/positive areal capacity ratio. With regard to full-cells using FP cathodes, it can be clearly seen that the cell using sodium mesoxalate and avoiding presodiation step (Figure 3d) presents higher specific capacities, with longer and higher voltage *plateaux*, and provides the same specific capacity values that were obtained in the cathode assessment, very close to the theoretical  $C_{sp}$  (130 mAh g<sup>-1</sup>) both for 9 and 26 mA g<sup>-1</sup> galvanostatic cycling.

**Figure 4** exhibits the charge–discharge curves of HC // NVP\_S and HC // FP\_S full-cells assembled with mass balances of 1.08 and 1.11 cycled from 1.00 to 4.20 V and 1.00 to 4.30 V at 9 mA g<sup>-1</sup> of together with the separated contributions of the electrodes (sunflower seed shells-derived HC as anode and NVP\_S and FP\_S as cathodes). As mentioned before, the initial cycle of the cells involved a constant potential stage at 4.20 V for 18 h to facilitate the decomposition of the sacrificial salt in the cathode, in addition to the formation of the solid electrolyte interphase on the anode.<sup>[12]</sup> In the case of HC // NVP\_S (Figure 4a,c), partial sacrificial salt decomposition is observed as a small *plateau* at 4.00 V versus Na<sup>+</sup>/Na in the 2nd to 3rd cycles, indicating that the decomposition of the remaining sodium mesoxalate in

the cathode continues during the 2nd cycle. This extension of the sodium mesoxalate degradation step is related to a slight imbalance of the sacrificial salt content with the constant voltage step length. Hence, it would be solved by using a longer constant voltage stage in the first cycle. Anyway, incomplete decomposition of the sacrificial salt only adds a small *plateau* at 4.00 V in the full-cell and does not affect the cell performance in terms of specific capacity, as the obtained  $C_{sp}$  values in cell discharge do not change in these cycles. Moreover, this system exhibits an inadequate N/P ratio, as the anode (Figure 4e) is significantly underutilized, achieving less than 50% of its practical specific capacity (Figure S1a, Supporting Information), which is primarily due to the anode's *plateau* being largely untapped. On the other hand, the cathode (Figure 4c) appears to only reach the end of its *plateau*.

In contrast, sodium mesoxalate was completely decomposed in HC // FP\_S battery after 18 h because no phenomenon was registered at high voltage from the 2nd to the 5th cycle. Analysis of the separate contributions of anode and cathode (Figure 4d,f) indicates that the selected N/P ratio was an optimal one, because the full-cell (Figure 4b) provided the practical specific capacity of the cathode in half-cell (Figure 2d). Moreover, the anode voltage profile shows that the specific capacity of the anode is supplied both by the sloppy and the low-voltage region of the hard carbon, which maximizes the cell practical operating voltage and power. The rate capabilities of NVP and FP presodiated full-cell chemistries and the full-cell systems containing

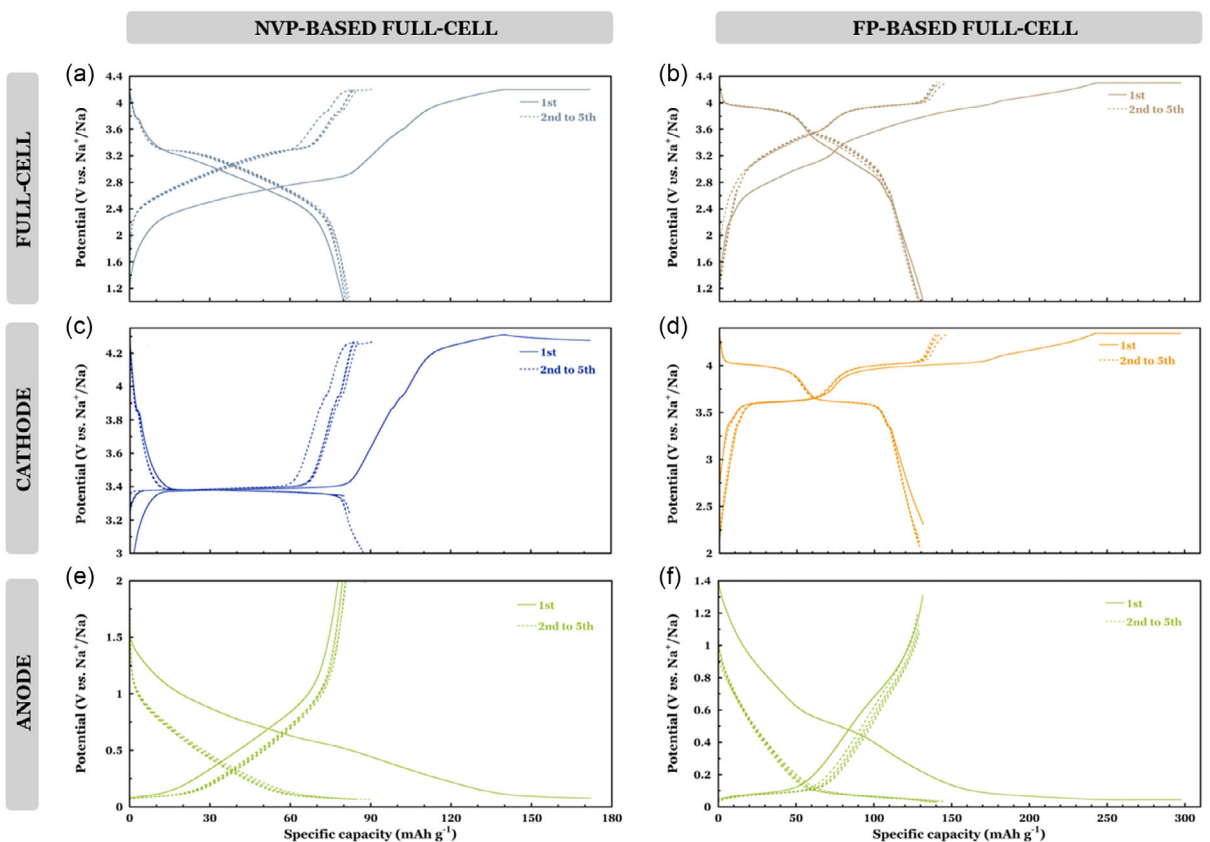


**Figure 4.** Voltage profile of the HC // NVP\_S and HC // FP\_S full-cells and the corresponding cathode and anode charge–discharge curves of a,c,e) 1.08 and b,d,f) 1.11 mass balances, respectively.

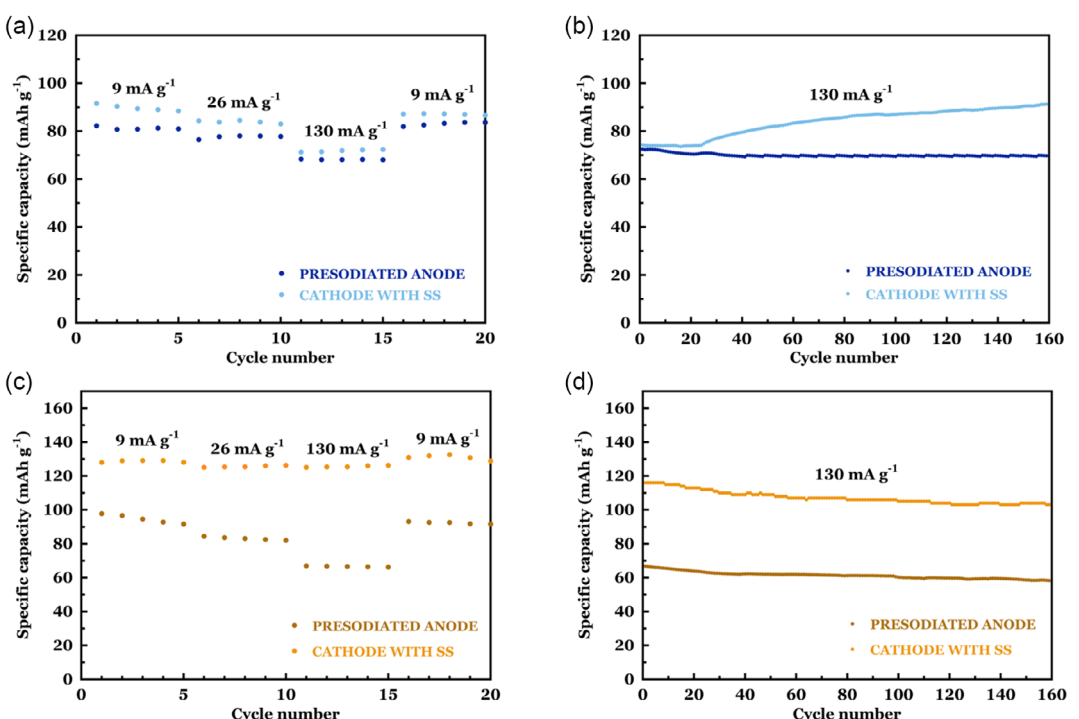


**Figure 5.** Discharge rate capabilities and cycle performances of a,b) HC // NVP and c,d) HC // FP with and without sacrificial salt, respectively.

sodium mesoxalate at different current densities are displayed in Figure 5a,c. Despite the relatively low-rate capabilities in both NVP full-cells (Figure 5a), the batteries exhibit a specific capacity retention of 83 % when going from 9 to 130 mAh g<sup>-1</sup>. The rate capability of the HC // FP presodiated full-cell battery (Figure 5c) at different current densities presents a specific capacity retention of 70% from 9 to 130 mA g<sup>-1</sup>, whereas this parameter of HC // FP\_S full-cell is outstanding, with very high  $C_{sp}$  retention when going from low-to-high rates.

Cyclability tests were conducted at high current density to assess the medium-term performance of all the full-cell batteries, as depicted in Figure 5b,d. The results indicate good stability in all the systems, presodiated and sacrificial salt ones for 160 cycles, which is consistent with the expected performance of polyanionic cathodes and also with the cyclability registered for the sunflower seed shell-derived anode. Nonetheless, in both HC // NVP and HC // FP full-cells, the use of sacrificial salt increases the  $C_{sp}$  from 70 to 95 mAh g<sup>-1</sup> and from 60 to 110 mAh g<sup>-1</sup>. HC // NVP\_S (Figure 5b) exhibited increasing specific capacity on the full-cell, with  $C_{sp}$  values ranging from 72 to 95 mAh g<sup>-1</sup>, which could correspond to electrochemical performance enhancement as possible remaining sacrificial salt is decomposed with extended cycling. Nonetheless, it can be said that during cyclability test at 130 mA g<sup>-1</sup>, the HC // NVP\_S full-cell presents good long-term cycling stability.

It must be noted that the number of studies of  $\text{Na}_3\text{V}_2(\text{PO}_4)_3@\text{C}$  as cathode and hard carbon as anode is considerably limited, compared to the number of publications about NASICON symmetrical cells, so little comparisons with literature can be established.<sup>[41,42]</sup> However it can be said that the obtained results from the electrochemical performances are adequate but still

significantly lower compared to the ones obtained for  $\text{Na}_3\text{V}_2(\text{PO}_4)_3@\text{C}$  with sacrificial salt cathode in half-cell configuration (95 mAh g<sup>-1</sup>). Hence, further optimization in terms of cathode formulation and N/P ratio is needed for these systems, but the feasibility of a not presodiated hard carbon-based Na-ion full-cell using a NASICON cathode has been demonstrated.

Additionally, the HC // FP\_S full-cell displays excellent long-term cycling stability at 130 mA g<sup>-1</sup> ( $\approx 110$  mAh g<sup>-1</sup> after 160 cycles with a capacity retention of  $\approx 92\%$ ). As it has been demonstrated, all the studied full-cells present outstanding stability, which is an expected feature of polyanionic cathodes, but in this case also demonstrates that biowaste-derived hard carbon can perform notably for very long, without limiting the battery performance. Thus, it can be said that HC // FP\_S system is fully compatible, that it is possible to assemble biomass-based sodium-ion full-cells with some cathode formulation modifications, and that these full-cells are robust in the long term. Therefore, commercial exploit of biomass-based hard carbons is possible by using a sacrificial salt as additive.

*Post-mortem* analysis of the electrodes cells was carried out in order to study, on the one hand, the surface of the cathodes with sodium mesoxalate in their composition and, on the other hand, the SEI formed on the two kinds of anodes, the presodiated ones and the ones where the extra  $\text{Na}^+$  ions were provided by sodium mesoxalate decomposition. The cells were disassembled in the glovebox and the electrodes were rinsed with propylene carbonate and dried under argon to ensure the removal of any salt deposits from the electrolyte on the electrodes. Figure 6 exhibits transverse section micrographs of negative (with or without presodiation step) and positive electrodes of both cathodes (NVP, NVP\_S, FP, and FP\_S) from the *post-mortem* cells after the cycling

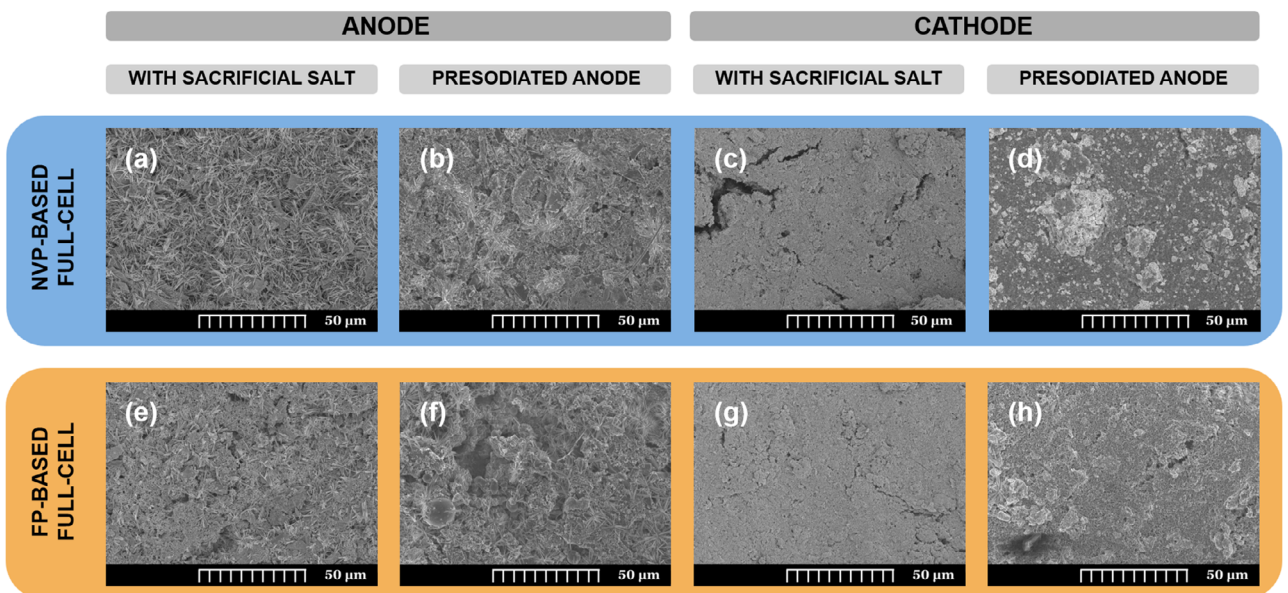


**Figure 6.** Surface morphology of the a,e) negative and c,g) positive electrodes with sacrificial salt of HC // NVP\_S and HC // FP\_S and b,f) presodiated anode and d,h) cathode materials of HC // NVP and HC // FP after 160 cycles, respectively.

protocol reached cycle 160. Two different structures appeared in the micrographs displayed in the anodes with or without a pre-cycling step of the full-cells. On the one side, fibers on the surface of the electrodes can be observed (Figure 6a,e,f), that come from the fiberglass separator and become stuck during the cycling process. On the other hand, needle-like crystals with a snowflake arrangement can be observed as shown in Figure 6b,f. These snowflake-like structures are related to a sodium-containing salt, as has been proved by EDX analysis on the samples. This suggests that they are crystallized NaPF<sub>6</sub> coming from the incomplete rinsing of the electrodes. No cracks are appreciated in the case of the anodes (Figure 6a,b,e,f), as could be expected, but some fractures and pores about 5 μm are clearly seen in the NVP\_S post-mortem electrode (Figure 6c), and smaller ones in the FP\_S post-mortem cathode (Figure 6g). These splits are related to the released gases during the decomposition of the sacrificial salt. Despite the presence of surface fractures, the electrodes maintain their electrochemical performance, as evidenced by the excellent cycle life previously shown in Figure 5b,d. In general, cathodes with sacrificial salt in their formulation exhibit a similar fractured structure with pores that can improve electrolyte access.<sup>[12]</sup> The size of these pores remains relatively constant despite repeated cycling, suggesting that they are formed during the initial decomposition of the sacrificial salt and subsequent gas release (Figure S2a and S2d, Supporting Information). Despite the observed fractures in the surface of sodium salt electrodes and the deterioration of both materials after cycling, the electrochemical performance remains stable after 160 cycles, which indicates that these structural microfailures were not significant to the cell operation.

The surface of the *post-mortem* electrodes was also analyzed by X-ray photoelectron spectroscopy (XPS). The C1s, O1s, and F1s photoelectron spectra of the anodes cycled after 160 cycles in full-cell with (HC // NVP\_S and HC // FP\_S) and without sacrificial salt (HC // NVP and HC // FP) are exhibited in Figure 7 and S3,

Supporting Information. In all the anodes, the C1s and O1s photoelectron spectra show a similar pattern, with very slight variations among the different relative signals. In both cases, with or without a precycling step, the C—C peak is attributed to the carbon, hydrogen, and oxygen content of the hard carbon active material. The O1s spectra show peaks corresponding to C=O and C—O functional groups with the same relative intensities for both postmortem anodes, which suggests that the same organic species have been formed on both kinds of anodes, presodiated and the ones using sodium mesoxalate in the cathode.

Furthermore, in all full-cell systems, F1s photoelectron spectra of the anodes exhibit two major peaks attributed to NaPF<sub>6</sub> or PVDF-derived species (687.50 eV) and NaF (684.60 eV). This latter contribution assigned to NaF in the anode from NVP and FP sacrificial salt-containing cells (1.88 at.% and 0.64 at.%) is lower than in precycled anode full cells (6.73 at.% and 1.53 at.%). The presence of NaF indicates degradation of NaPF<sub>6</sub> but depending on the proportion and its distribution, it is considered that it can favor Na<sup>+</sup> diffusion through the SEI.<sup>[43]</sup> Further XPS studies should be carried out in order to determine the full structure of the SEI in these presodiated and sacrificial salt anodes. To sum up, the overall patterns observed in the C1s and O1s spectra of anodes are similar, with comparable contributions from the same species, but with slightly different species distribution on the F1s spectrum. Therefore, the surface of the SEI that is generated by using sodium mesoxalate as sacrificial salt is very similar to the one generated by presodiating the anode before full-cell assembly, but depth profile XPS study would be needed to analyze the full SEI structure.

The C1s, F1s, and O1s photoelectron spectra of the HC // NVP\_S, HC // FP\_S, HC // NVP, and HC // FP cathodic materials are displayed in Figure 8 and S4, Supporting Information. In general, NVP and FP with and without sodium salt chemistries exhibit similar peaks in C1s and O1s spectra, which are related to the carbon present in the cathode formulation. The F1s photoelectron spectra of the

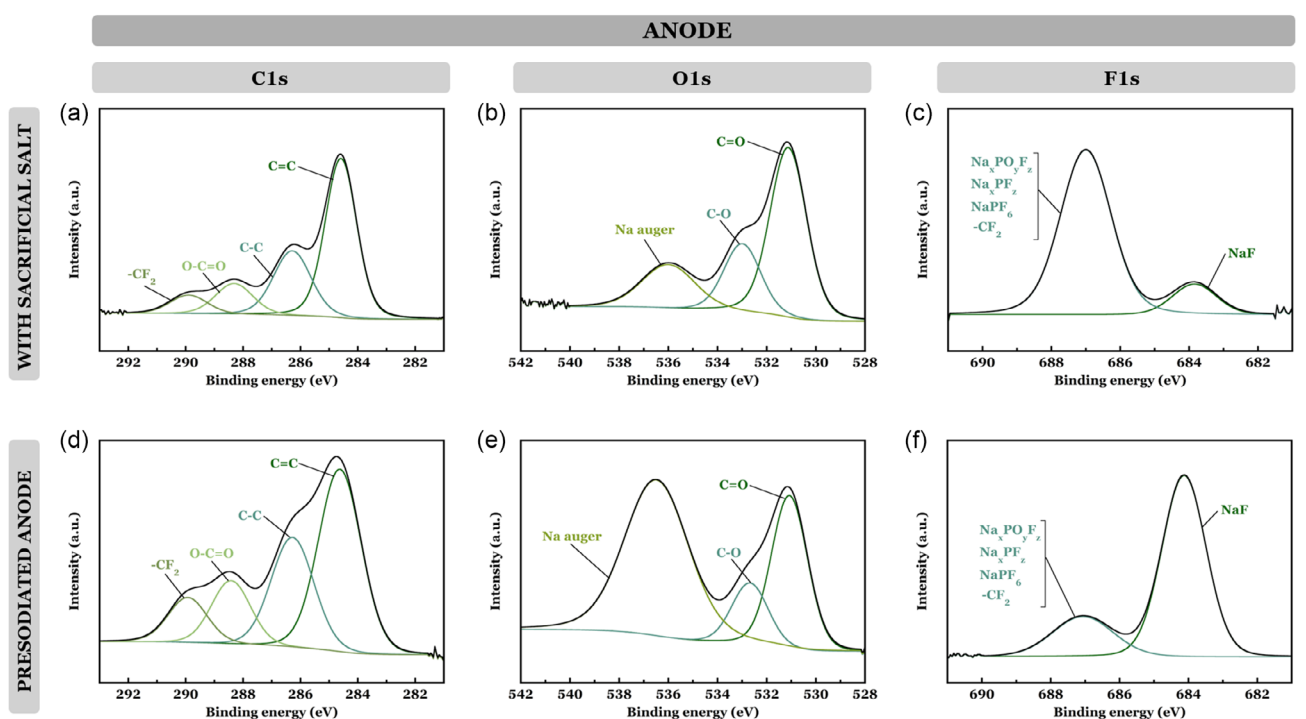


**Figure 7.** a,d) C1s, b,e) O1s, and c,f) F1s photoelectron spectra of the post-mortem anodes without precycling step (HC // NVP\_S) and with presodiation (HC // NVP) of NVP full-cells, respectively.

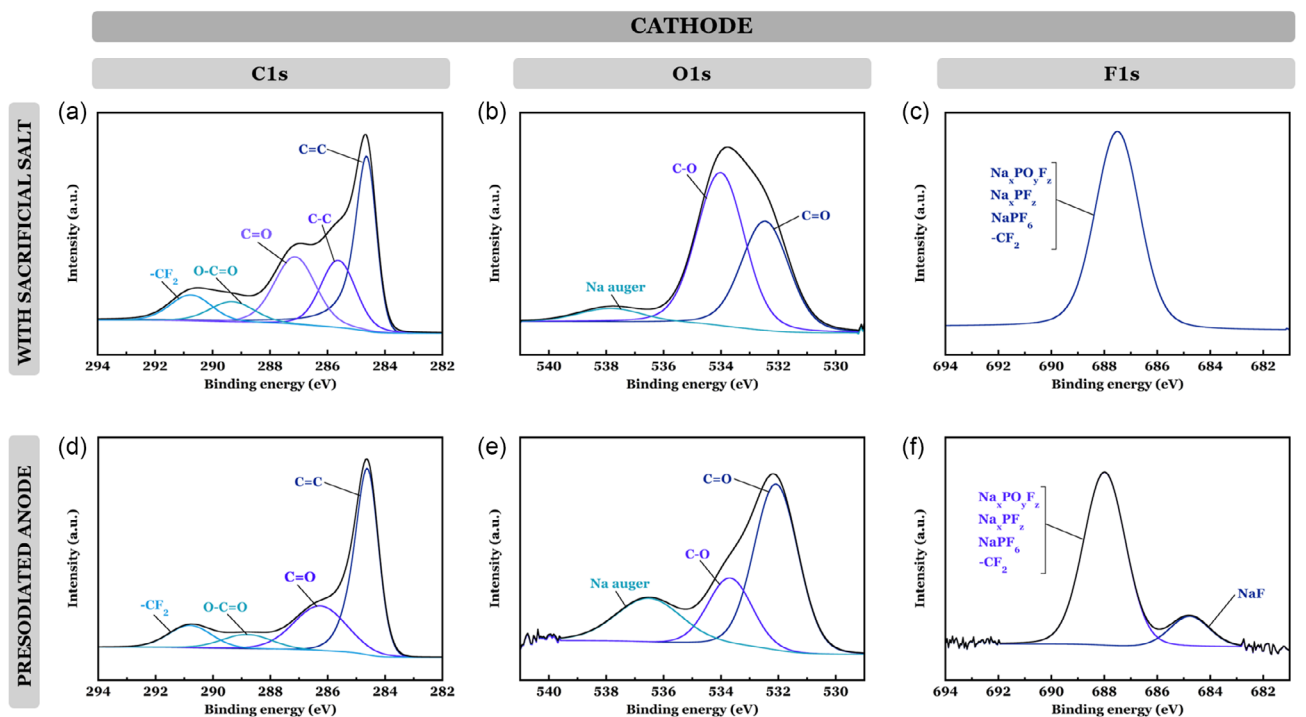


**Figure 8.** a,d) C1s, b,e) O1s, and c,f) F1s photoelectron spectra of the post-mortem cathodes containing sacrificial salt (HC // NVP\_S) and without the additive (HC // NVP) of NVP full-cells, respectively.

HC // NVP\_S HC // FP\_S and HC // FP cathodes (Figure 8c, S4c and S4f, Supporting Information) exhibit a single peak at 687.80 eV, which is attributed to fluorinated species from the PVDF electrode coating or to NaPF<sub>6</sub> electrolyte salt. On the contrary, HC // NVP (Figure 8f) exhibits an additional peak that can be assigned to

NaF. This fact indicates a higher degree of electrolyte degradation for the full-cell without sacrificial salt.

To complete the evaluation of the viability of different full-cell systems based on sunflower seed shells-derived hard carbon combined with two polyanionic cathode chemistries, a Life Cycle

**Table 1.** Normalized impact values for the two studied battery systems. The significance of the shaded cells is to help the reader differ easily between the two battery systems (NVP = blue and FP = orange). While bold data is to highlight one of the most interesting parameters of the LCA.

Indicator	Unit	NVP_S BATTERY	FP_S BATTERY
Fine particulate matter formation	kg PM2.50 eq	1.28 E-12	1.11 E-13
Fossil resource scarcity	kg oil eq	2.25 E-10	1.93 E-11
Freshwater ecotoxicity	kg 1.40-DCB	8.69 E-11	7.42 E-12
Freshwater eutrophication	kg P eq	8.29 E-13	7.05 E-14
Global warming	<b>kg CO<sub>2</sub> eq</b>	<b>8.39 E-10</b>	<b>7.20 E-11</b>
Human carcinogenic toxicity	kg 1.40-DCB	6.92 E-11	6.11 E-12
Human noncarcinogenic toxicity	kg 1.40-DCB	1.23 E-09	1.05 E-10
Ionizing radiation	kBq Co-60 eq	4.18 E-10	3.55 E-11
Land use	m2a crop eq	2.05 E-11	2.08 E-12
Marine ecotoxicity	kg 1.40-DCB	1.09 E-10	9.34 E-12
Marine eutrophication	kg N eq	5.97 E-14	5.20 E-15
Mineral resource scarcity	kg Cu eq	1.71 E-12	1.55 E-13
Ozone formation (human health)	kg NO <sub>x</sub> eq	1.56 E-12	1.36 E-13
Ozone formation (terrestrial ecosystems)	kg NO <sub>x</sub> eq	1.57 E-12	1.37 E-13
Stratospheric ozone depletion	kg CFC-11 eq	3.94 E-16	3.38 E-17
Terrestrial acidification	kg SO <sub>2</sub> eq	3.17 E-12	2.73 E-13
Terrestrial ecotoxicity	kg 1.40-DCB	9.02 E-10	7.89 E-11
Water consumption	m <sup>3</sup>	1.41 E-11	1.21 E-12

Assessment (LCA) analysis of the batteries containing sacrificial salt was been performed. In order to compare the impacts obtained for each full-cell, NVP-based and FP-based, the obtained impacts were normalized by using **Formula 1**

#### Normalized impact

$$\text{Impact value} = \frac{\text{impact}}{[\text{Battery energy density (Wh} \cdot \text{kg)} \cdot \text{cathode active mass(kg)}]} \quad (1)$$

$$= \frac{\text{impact}}{\text{Wh}}$$

As the specific capacity values for the cells have been presented per gram of cathode active mass, the LCA normalization has followed the same criteria. The normalized impact values for each full-cell chemistry are gathered in **Table 1**.

In order to compare the relative footprint of each cell chemistry, **Figure 9** shows the relative contribution of each system to the 18 selected impact categories. As it can be seen, the footprint of the battery using NVP\_S cathode is about 9 times higher than the full-cell using FP\_S cathode in all category impacts. Considering global warming as the most relevant category regarding the “Neat zero carbon” objectives for 2050, a more thorough study was made in Global Warming Potential category by analyzing and comparing the main contributions to this category of each battery element (cathode, anode, metal casing, and electrolyte) of both cell chemistries.<sup>[44,45]</sup> **Figure 10** shows this distribution for the main contributions for each system,

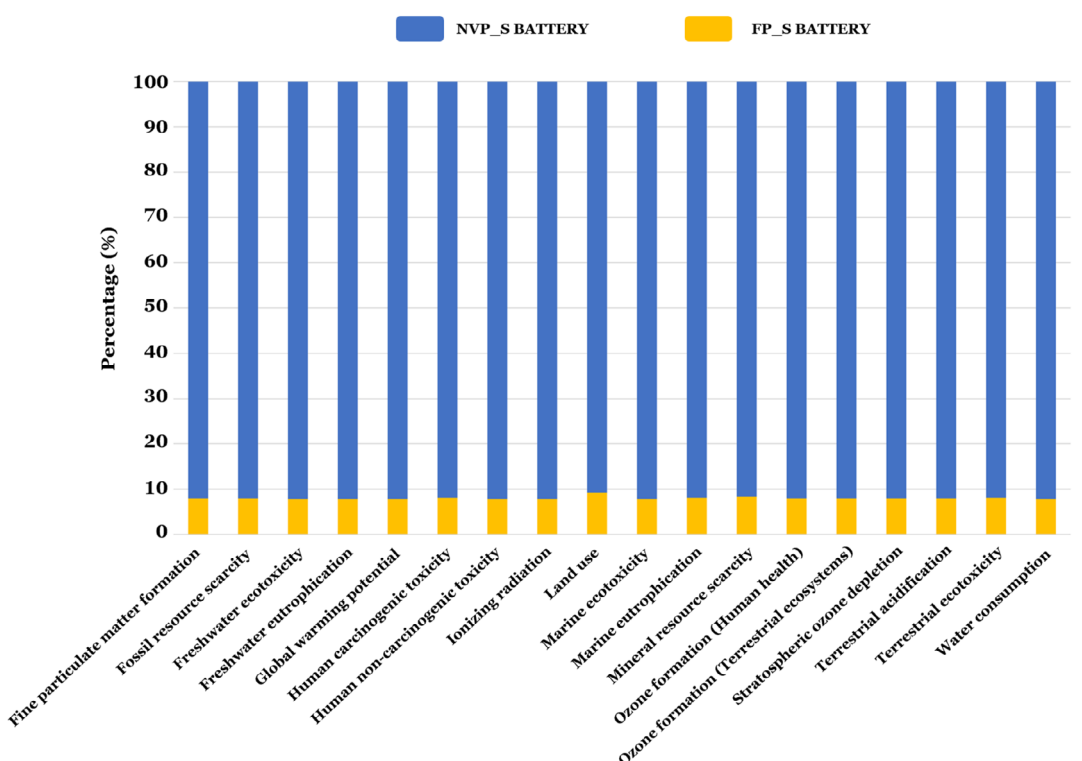


**Figure 9.** Relative contribution of the two full-cells prepared by using sodium mesoxalate as cathode additive to the selected 18 environmental impact categories.

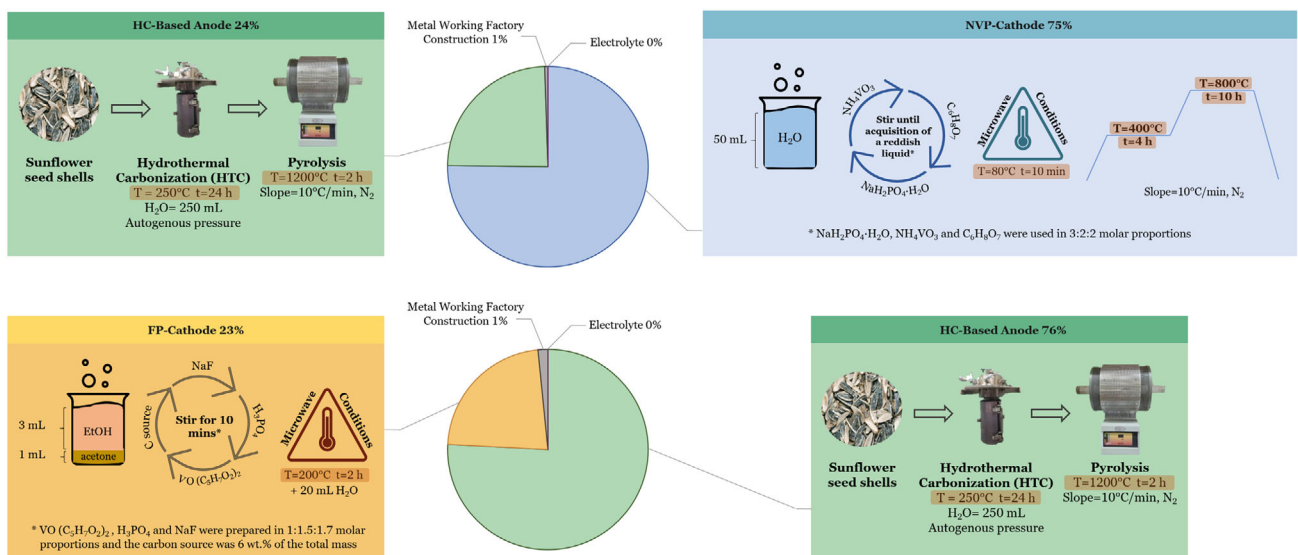


Figure 10. Relative contribution of the battery elements to Global Warming Potential for each full-cell chemistry, together with synthetic procedures involved in their preparation. Steps considered as energy-consuming ones are highlighted in orange.

together with the synthetic procedures involved for each battery element.

The analysis of the graphics in Figure 10 shows great differences between the two systems, while for NVP\_S-based full cell the main contribution to Global Warming Potential comes from the cathode material, the battery using FP\_S shows the opposite trend, with the anode material as the principal source of  $\text{CO}_2$ . This difference can be understood by comparing the preparative routes followed for each material and the electricity expense in each case. The anode material is the same in both batteries, obtained from biomass (sunflower seed shells) by a hydrothermal carbonization step and further pyrolysis at 1200 °C for 2 h.<sup>[9]</sup> This latter pyrolysis step, despite not being very long, involves the use of a very high temperature, which entails high energy expense. The energy needed to produce the NVP active material, besides, seems to exceed the one needed by the anode, as can be deduced from the diagram. In this case, two subsequent thermal treatments at 400 and 800 °C of 4 and 10 h, respectively, must be used to produce this active material. Thus, despite the lower treatment temperature, more energy is consumed to produce the necessary NVP material compared to the one needed for the biomass-based anode (Figure 10).

In addition, when analyzing FP\_S-based full-cell, the anode is the most energy-consuming element in the set. This is due to the milder synthetic conditions of the fluorophosphate material, which only involves a low-temperature microwave treatment for 2 h. Thus, it can be said that, considering the two full-cell chemistries, the biomass-based HC // FP\_S battery presents not only the best electrochemical performance in terms of stored specific capacity and cycle life, but also can make a difference in terms of environmental footprint.

### 3. Conclusion

In this work, it has been demonstrated that it is possible to directly assemble fully functional hard carbon-based Na-ion batteries by

using sodium mesoxalate as a cathode additive with two poly-anionic cathode chemistries:  $\text{Na}_3\text{V}_2(\text{PO}_4)_3@\text{C}$  and  $\text{Na}_3\text{V}_2\text{O}_2(\text{PO}_4)_2\text{F}@\text{C}$ . While the cathode formulation for NVP\_S cathodes needs further optimization to get optimized results, FP\_S system exhibited satisfactory rate capability at moderate-to-high current densities and an extremely robust stability after 1000 cycles. Post-mortem analysis of the cycled electrodes both in presodiated and sacrificial salt-containing cells showed cracks in the cycled cathodes containing sodium mesoxalate but without any sign of decline in cyclability. Moreover, it was proved that the SEI generated using the sacrificial salt was comparable to the one formed during the presodiation process. Additionally, LCA calculations on both cathode chemistries containing the sacrificial salt indicated that the FP\_SS cathode presented lower environmental impact compared to the NVP\_S electrode. Therefore, it can also be suggested that LCA methodology should be used for decision-making during design processes. To sum up, it can be said that HC // FP\_S full-cell has been optimized with the proper mass balance to get good electrochemical performance, similar to the expected one for the cathode in half-cells. The combination of the optimized biowaste-derived hard carbon anode with FP-cathode has led to a robust sodium-ion battery that avoids presodiation step and puts these systems closer to their industrial deployment. Hence, a future with greener and more environmentally friendly materials for Na-ion batteries is possible.

## 4. Experimental Section

### Sacrificial Sodium Salt Preparation

Anhydrous sodium mesoxalate ( $\text{Na}_2\text{C}_3\text{O}_5$ ) was obtained by dehydrating sodium mesoxalate monohydrated ( $\text{Na}_2\text{C}_3\text{O}_5 \cdot \text{H}_2\text{O}$ , white solid, Sigma-Aldrich, 98%) at 200 °C under vacuum for 12 h, resulting in a yellowish solid. This salt was then combined with Ketjen black (KB) in a 70:30 weight ratio to form a composite additive for cathode electrodes. Ketjen black was chosen as the conductive

agent due to its high specific surface area, which is crucial for overcoming the insulating nature of the sacrificial salt (SS), favoring the oxidation of the sacrificial salt, leading to an efficient supply of  $\text{Na}^+$  ions for the anode and, thus, maximizing electrode performance, as supported by existing literature.<sup>[12]</sup> This mixture was labeled as KB + SS and it was used for positive electrode preparation. This mixture was made and preserved inside the glovebox to avoid water intake from sodium mesoxalate.

### Cathode Synthesis

$\text{Na}_3\text{V}_2(\text{PO}_4)_3@\text{C}$  (NVP) material was prepared by a two-step synthesis. The first part consisted of mixing stoichiometric ratios of  $\text{NaH}_2\text{PO}_4 \cdot \text{H}_2\text{O}$ ,  $\text{NH}_4\text{VO}_3$ , and  $\text{C}_6\text{H}_8\text{O}_7$  (Sigma-Aldrich) in 50 mL of water, which was introduced into a Teflon vessel of a microwave reactor (CEM MARS 5 230/60) at 80 °C for 20 min. Subsequently, the mixture was filtered and dried at 80 °C to afterwards anneal it twice under nitrogen atmosphere at 400 °C for 4 h and 800 °C for 10 h with a heating rate of 10 °C min<sup>-1</sup>. On the other hand, the  $\text{Na}_3\text{V}_2\text{O}_2(\text{PO}_4)_2\text{F}@\text{C}$  (FP) composite was synthesized by a microwave-assisted hydrothermal method. First, 7 mL of ethanol mixed with 3 mL of acetone was poured into the vessel followed by  $\text{VO}(\text{C}_5\text{H}_7\text{O}_2)_2$ ,  $\text{H}_3\text{PO}_4$ , and NaF in stoichiometric ratio with a 6% molar excess of Ketjen Black. Afterward, 60 mL of water was added to the mixture and all the reactants were stirred for 10 min. This suspension was introduced in the Teflon vessel of a microwave reactor (CEM MARS 5 230/60) at 200 °C for 2 h. It was subsequently filtered with distilled water and acetone, followed by drying the mixture in a vacuum oven at 80 °C overnight. The carbon content of NVP and FP composite materials was determined to be 7 wt.% and 14 wt.% through elemental analysis, respectively.

### Anode Synthesis

Hard carbon anodes were prepared from sunflower seed shells for this study. The synthesis method was reported in previous work.<sup>[9]</sup>

### Physicochemical Characterization

The obtained materials were characterized by XRD, scanning electron microscopy (SEM), and XPS. X-ray diffraction was carried out in a PANalytical Xpert PRO diffractometer with Cu-K $\alpha$  radiation source ( $\lambda = 1.5418 \text{ \AA}$ ). The morphology of the resulting materials was observed by scanning electron microscopy with Hitachi S-4800 equipment. XPS was performed on a Thermo ESCALAB250Xi spectrometer with monochromatic Al-K $\alpha$  source.

### Electrode Preparation

In the case of the cathodes, two types of electrodes were prepared, conventional ones, containing the active material, conductive additive, and binder, and the ones comprising sodium mesoxalate. For the conventional cathodes, both  $\text{Na}_3\text{V}_2(\text{PO}_4)_3@\text{C}$  and  $\text{Na}_3\text{V}_2\text{O}_2(\text{PO}_4)_2\text{F}@\text{C}$  electrodes (NVP and FP) were processed by mixing active material, conductive carbon black (C65), and polyvinylidene fluoride (PVDF) at a mass ratio of 8:1:1 using N-methyl-2-pyrrolidone (NMP) as the solvent. On the other hand, the positive electrodes containing sacrificial salt (NVP\_S and FP\_S) were prepared by mixing the active material, conductive carbon black, PVDF, and KB + SS at a mass ratio of 6.667:0.833:0.833:1.667 using NMP as the solvent. Additionally, FP\_S electrode formulation mass ratio was 5.714:0.714:0.714:2.858. Hard carbon-based anodes comprised 80 wt.% of active material derived from sunflower seed shells, 10 wt.% conductive carbon black, and 10 wt.% polyvinylidene fluoride binder using NMP as the solvent. In all cases, aluminum foil was used as the current collector and the electrodes were punched out with diameters of 16 mm.

### Electrochemical Characterization

CR2032-type coin cells were used to assess the electrochemical performance of the cathodes and the recycling step for half-cell measurements. They were assembled in an Ar-filled glove Box, where glass microfiber filters (Whatman GF/A, thickness of 260  $\mu\text{m}$ ) were used as separators and metallic sodium as counter electrode. In the case of the presodiated full cells, the 2032 half-cells were disassembled after cycling and the presodiated anodes were paired with the corresponding cathode. The three-electrode EL-cells (PAT-cells) used for full-cell measurements were assembled in Ar-filled glove Box. Glass microfiber filters (Whatman GF/D, thickness of 260  $\mu\text{m}$ ) were used as separators, hard carbon electrodes were used as counter electrodes, and sodium metal was used as reference electrode. In all measurements, the amount of electrolyte used in each cell was 150  $\mu\text{L}$  of a 1 M  $\text{NaPF}_6$  solution in ethylene carbonate/propylene carbonate (EC/PC, 1:1 in volume). All electrochemical measurements were carried out on a multichannel potentiostat/galvanostat (Biologic VMP3) at room temperature. In NVP and FP, the voltage window ranged between 2.30–3.90 V and 2.50–4.30 V, respectively, for half cells, whereas it was extended to 1.00–4.20 V and 1.00–4.30 V for full-cells. In the case of NVP\_S and FP\_S, after reaching 4.20 or 4.30 V in the first charge, the potential was maintained at this value for 18 h, in both half- and full-cell measurements, to ensure that the sacrificial salt was fully decomposed. For the anode presodiation, the recycling protocol was performed between 0.002 and 2.00 V cycling the half-cell three times at a current density of 9 mA g<sup>-1</sup> and finishing in the oxidized state.

### Life Cycle Assessment

LCA methodology was applied according to ISO 14040. OpenLCA 2.3 software and ecoinvent v3.10 database were used. The environmental impact calculation was done using Recipe 2016 Midpoint H methodology, where 18 environmental impact categories are measured, and for this research, a special focus on Global warming category was made. The system boundary was from cradle to manufacturing. The functional unit (FU) selected to carry out the analysis was defined as manufacturing one battery cell per real Wh. To fulfill the inventory for the LCA, mainly primary data from the laboratory was used. Finally, to thoroughly assess the complete environmental impact of the full-cells containing a sacrificial salt, two scenarios were considered: HC // NVP\_S and HC // FP\_S batteries.

### Acknowledgements

This work was financially supported by the Ministerio de Ciencia e Innovación (PID2023-151153OB-I00) and Gobierno Vasco/Eusko Jaurlaritza (IT-1226-19 and IT-1554-22). The authors would also like to thank the technical and human support provided by SGIker of UPV/EHU.

Open Access funding enabled and organized by Projekt DEAL.

### Conflict of Interest

The authors declare no conflict of interest

### Data Availability Statement

The data that support the findings of this study are available on request from the corresponding author. The data are not publicly available due to privacy or ethical restrictions.

**Keywords:** biowaste-based hard carbon · Na-ion full-cells · polyanionic compounds · sodium mesoxalate

- [1] HiNa. HiNa Battery Technology Co. <https://www.hinabattery.com/en/> (accessed July 2024).
- [2] CATL. Contemporary Amperex Technology (CATL). <https://www.catl.com/es/> (accessed May 2024).
- [3] Tiamat. Tiamat. <https://www.tiamat-energy.com/> (accessed May 2024).
- [4] Natron Energy. Natron Energy Inc. <https://natron.energy/> (accessed May 2024).
- [5] Faradion Ltd. Faradion Ltd. <https://faradion.co.uk/> (accessed May 2024).
- [6] Y. Chu, J. Zhang, Y. Zhang, Q. Li, Y. Jia, X. Dong, J. Xiao, Y. Tao, Q. H. Yang, *Advanced Materials*. **2023**, *35*, 2212186.
- [7] Y. Huang, Z. Tang, S. Zhou, H. Wang, Y. Tang, D. Sun, H. Wang, *J. Phys. D: Appl. Phys.* **2022**, *55*, 313002.
- [8] L. Liu, H. R. Tinker, Y. Wu, J. Lv, L. Li, Y. Fang, Y. Wu, Y. Xu, *Mol. Syst. Des. Eng.* **2024**, *9*, 660.
- [9] N. Nieto, J. Porte, D. Saurel, L. Djuandhi, N. Sharma, A. Lopez-Urionabarrenechea, V. Palomares, T. Rojo, *ChemSusChem* **2023**, *16*, e202301053.
- [10] J. Martínez De llarduya, L. Otaegui, M. Galcerán, L. Acebo, D. Shanmukaraj, T. Rojo, M. Armand, *Electrochim. Acta* **2019**, *321*, 134693.
- [11] D. Shanmukaraj, K. Kretschmer, T. Sahu, W. Bao, T. Rojo, G. Wang, M. Armand, *ChemSusChem* **2018**, *11*, 3286.
- [12] A. J. Fernández-Ropero, M. Zarrabeitia, G. Baraldi, M. Echeverria, T. Rojo, M. Armand, D. Shanmukaraj, *ACS Appl. Mater. Interfaces* **2021**, *13*, 11814.
- [13] K. Liu, Y. Liu, D. Lin, A. Pei, Y. Cui, *Sci. Adv.* **2018**, *4*, eaas9820.
- [14] Y. Li, X. Feng, D. Ren, M. Ouyang, L. Lu, X. Han, *ACS Appl. Mater. Interfaces* **2019**, *11*, 46839.
- [15] T. Song, Y. Chen, L. Chen, E. Kendrick, *J. Power Sources* **2024**, *624*, 235599.
- [16] G. Mu, S. Agrawal, P. Sittisomwong, P. Bai, *Electrochim. Acta* **2022**, *406*, 139878.
- [17] Y. Abe, S. Kumagai, *J. Energy Storage* **2018**, *19*, 96.
- [18] Y. Sun, S. Guo, H. Zhou, *Adv. Energy Mater.* **2019**, *9*, 1800212.
- [19] Y. Liu, N. Zhang, F. Wang, X. Liu, L. Jiao, L. Z. Fan, *Adv. Funct. Mater.* **2018**, *28*, 1801917.
- [20] Y. Niu, Y. Zhang, M. Xu, *J. Mater. Chem. A. Royal Soc. Chem.* **2019**, *7*, 15006.
- [21] S. P. Guo, J. C. Li, Q. T. Xu, Z. Ma, H. G. Xue, *J. Power Sources* **2017**, *361*, 285.
- [22] H. Rostami, J. Valio, P. Suominen, P. Tynjälä, U. Lassi, *Chem. Eng. J.* **2024**, *495*, 153471.
- [23] T. Yin, Z. Zhang, L. Xu, C. Li, D. Han, *ChemistryOpen* **2024**, *13*, e202300178.
- [24] E. Marelli, C. Marino, C. Bolli, C. Villevieille, *J. Power Sources* **2020**, *450*, 227617.
- [25] J. Martínez De llarduya, L. Otaegui, J. M. López del Amo, M. Armand, G. Singh, *J. Power Sources* **2017**, *337*, 197.
- [26] G. Singh, B. Acebedo, M. C. Cabanas, D. Shanmukaraj, M. Armand, T. Rojo, *Electrochim. Commun.* **2013**, *37*, 61.
- [27] L. Zhang, B. Xiong, S. Gao, J. Li, D. Li, W. Deng, H. Hou, G. Zou, X. Ji, *Chem. Commun.* **2025**, *61*, 5386.
- [28] C. Lee, M. Shimizu, R. Tatara, K. Nakamoto, T. Hosaka, Z. T. Gossage, S. Komaba, *ACS Appl. Energy Mater.* **2025**, *8*, 5867.
- [29] B. Zhang, R. Dugas, G. Rousse, P. Rozier, A. M. Abakumov, J. M. Tarascon, *Nat. Commun.* **2016**, *7*, 10308.
- [30] X. Chen, Y. Zheng, W. Liu, C. Zhang, S. Li, J. Li, *Nanoscale* **2019**, *11*, 22196.
- [31] M. Iturrondobeitia, C. Vallejo, M. Berroci, O. Akizu-Gardoki, R. Minguez, E. Lizundia, *ACS Sustain. Chem. Eng.* **2022**, *10*, 9798.
- [32] I. Rey, C. Vallejo, G. Santiago, M. Iturrondobeitia, E. Lizundia, *ACS Sustain. Chem. Eng.* **2021**, *9*, 14488.
- [33] M. Iturrondobeitia, O. Akizu-Gardoki, R. Minguez, E. Lizundia, *ACS Sustain. Chem. Eng.* **2021**, *9*, 7139.
- [34] M. Iturrondobeitia, O. Akizu-Gardoki, O. Amondarain, R. Minguez, E. Lizundia, *Adv. Sustain. Syst.* **2022**, *6*, 2100308.
- [35] I. Rey, M. Iturrondobeitia, O. Akizu-Gardoki, R. Minguez, E. Lizundia, *Adv. Energy Sustainability Res.* **2022**, *3*, 2200049.
- [36] P. Feng, W. Wang, K. Wang, S. Cheng, K. Jiang, *J. Mater. Chem. A Mater.* **2017**, *5*, 10261.
- [37] P. Babbar, A. Ivanishchev, A. Churikov, A. Dixit, *Ionics* **2017**, *23*, 3067.
- [38] J. Li, G. Du, T. Huang, F. Zhang, M. Xie, Y. Qi, S. J. Bao, M. Xu, *Energy Technol.* **2020**, *8*, 2000494.
- [39] R. Liu, H. Liu, T. Sheng, S. Zheng, G. Zhong, G. Zheng, Z. Liang, G. F. Ortiz, W. Zhao, J. Mi, Y. Yang, *ACS Appl. Energy Mater.* **2018**, *1*, 3603.
- [40] Z. Lv, M. Ling, M. Yue, X. Li, M. Song, Q. Zheng, H. Zhang, *J. Energy Chem.* **2021**, *55*, 361.
- [41] P. Stüble, C. Müller, J. Klemens, P. Scharfer, W. Schabel, M. Häringer, J. R. Binder, A. Hofmann, A. Smith, *Batter. Supercaps.* **2024**, *7*, e202300375.
- [42] M. Sharma, R. S. Dhaka, *Indian J. Pure Appl. Phys.* **2024**, *62*, 93.
- [43] Z. Tang, H. Wang, P. F. Wu, S. Y. Zhou, Y. C. Huang, R. Zhang, D. Sun, Y. G. Tang, H. Y. Wang, *Angew. Chem. Int. Ed.* **2022**, *61*, e202200475.
- [44] United Nations. Climate Change Net Zero Coalition. [www.un.org/en/climatechange/net-zero-coalition](http://www.un.org/en/climatechange/net-zero-coalition) (accessed March 2025).
- [45] European Commission. 2050 long-term strategy. [climate.ec.europa.eu/eu-action/climate-strategies-targets/2050-long-term-strategy\\_en](http://climate.ec.europa.eu/eu-action/climate-strategies-targets/2050-long-term-strategy_en) (accessed March 2025).

Manuscript received: April 2, 2025

Revised manuscript received: June 3, 2025

Version of record online: